Evaluating energy efficiency in anaerobic membrane bioreactors: Effect of filtration/backwash cycle duration on net energy balance

Aymen Chaaben, Farshid Pajoum Shariati, Geoffroy Lesage, Jérôme Harmand, Marc Heran

Bioresource Technology 447 (2026) 134229

Contents lists available at ScienceDirect

Bioresource Technology

journal homepage: www.elsevier.com/locate/biortech

Evaluating energy efficiency in anaerobic membrane bioreactors: Effect of filtration/backwash cycle duration on net energy balance

Aymen Chaaben [a,b,*], Farshid Pajoum Shariati [b], Geoffroy Lesage [b], Jérôme Harmand [a], Marc Heran [b]

[a] Laboratory of Environmental Biotechnology (LBE), National Research Institute for Agriculture, Food and Environment (INRAE), 11100 Narbonne, France
[b] European Institute for Membranes (IEM), University of Montpellier 34000 Montpellier, France

HIGHLIGHTS

- Upgraded dynamic model combining anaerobic kinetics, fouling and biomass detachment.
- Accurate prediction of substrates, SMP, CH_4 production, and TMP.
- Effect of cycle duration on methane yield, fouling intensity, and net energy balance.
- Control of fouling and support longer membrane lifespan under optimal strategy.

GRAPHICAL ABSTRACT

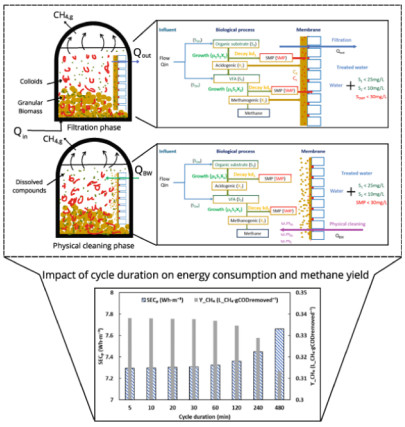

ARTICLE INFO

Keywords:
Membrane fouling
Granular sludge
Soluble microbial products
Anaerobic digestion
Dynamic modeling
Operational optimization

ABSTRACT

In this study, a dynamic model based on the AM2b anaerobic digestion framework was modified to simulate an anaerobic membrane bioreactor, including the return of detached biomass to the bioreactor bulk during physical backwashing. The identified model accurately captured the evolution of soluble microbial products, achieving a determination coefficient of 0.88, and its relevance was further confirmed through a post-operation characterization of the fouling layer, with relative errors between predicted and measured transmembrane pressures ranging from only 3.2% to 16.6% following refinement of fouling-related parameters. Then, the model was used to optimize the net energy balance (NEB) by simulating scenarios operated at filtration/backwash cycle durations (T_{cyc}) ranging from 5 min to 8 h. Results indicate that while total energy consumption remains relatively stable, methane production and NEB are affected by cycle duration. Longer cycles result in decreased biogas recovery due to membrane fouling and reduced microbial activity. Although the permeate pump represents only 6% of total energy use, its contribution increases slightly with extended cycles. The NEB reaches its maximum at short

* Corresponding author at: 300 avenue du Prof. Emile Jeanbrau, 34090 Montpellier France.
E-mail addresses: aymen.chaaben@inrae.fr (A. Chaaben), farshid.pajoumshariati@umontpellier.fr (F. Pajoum Shariati), geoffroy.lesage@umontpellier.fr (G. Lesage), jerome.harmand@inrae.fr (J. Harmand), marc.heran@umontpellier.fr (M. Heran).

https://doi.org/10.1016/j.biortech.2026.134229
Received 8 December 2025; Received in revised form 13 February 2026; Accepted 13 February 2026
Available online 15 February 2026

cycles (5–10 min) and declines progressively, with losses of up to 9% at 8-hour cycles. These results underscore the critical role of T_{cyc} optimization and the underlying attachment–detachment dynamics of the fouling layer.

Nomenclature

Parameter	Description
AnMBR	Anaerobic Membrane BioReactor
ADM1	Anaerobic Digestion Model N°1
AM2	Anaerobic digestion Model N°2
AM2b	Anaerobic digestion Model N°2 with SMP dynamics
A_0	Entire membrane surface (m^2)
A(t)	Dynamic of filter surface (m^2)
b_1	Yield of degradation of SMP by X_1 (−)
b_2	Yield of production of S_2 from SMP (−)
b_3	Yield of production of SMP from S_1 (−)
b_4	Yield of production of SMP from S_2 (−)
COD	Chemical Oxygen Demand
$C^G_{CH_4}$	Methane concentration in the gas phase ($mg{\cdot}L^{-1}$)
$C^L_{CH_4}$	Dissolved methane concentration in the liquid phase ($mg{\cdot}L^{-1}$)
C_S	Attachment coefficient of substrates (−)
C_{SMP}	Attachment coefficient of SMP (−)
C_X	Attachment coefficient of biomass (−)
DWWT	Domestic WasteWater Treatment
G-AnMBR	Granular Anaerobic Membrane BioReactor
J_P	Applied filtration volumetric flux ($L{\cdot}m^{-2}{\cdot}h^{-1}$)
$J_{P20,net}$	Permeate volumetric flux at T = 20 °C ($L{\cdot}m^{-2}{\cdot}h^{-1}$)
J_{BW}	Applied physical cleaning volumetric flux ($L{\cdot}m^{-2}{\cdot}h^{-1}$)
k_1	Yield of degradation of S_1 by X_1 (−)
k_2	Yield of production of S_2 from S_1 (−)
k_3	Yield of degradation of S_2 by X_2 (−)
k_4	Yield for CO_2 production by S_1 degradation ($L{\cdot}gCOD^{-1}$)
k_5	Yield for CO_2 production by S_2 degradation ($L{\cdot}gCOD^{-1}$)
k_6	Yield production of methane ($L\text{-}CH_4{\cdot}gCOD^{-1}$)
K_1	half-saturation constant associated with S_1 ($g{\cdot}L^{-1}$)
K_2	half-saturation constant associated with S_2 ($g{\cdot}L^{-1}$)
K_3	half-saturation constant associated with SMP ($g{\cdot}L^{-1}$)
K_i	inhibition constant associated with S_2 ($g{\cdot}L^{-1}$)
k_{d1}	Decay rate of the biomass X_1 (h^{-1})
k_{d2}	Decay rate of the biomass X_2 (h^{-1})
m_c	Cake layer mass (g)
$\overline{m}$	Optimal mass of cake layer (g)
NEB	Net Energy Balance ($Wh{\cdot}m^{-3}$)
OLR	Organic Loading Rate ($kgCOD{\cdot}m^{-3}{\cdot}d^{-1}$)
Q_{in}	Feed flow rate ($L{\cdot}h^{-1}$)
Q_{out}	Outlet flow rate ($L{\cdot}h^{-1}$)
Q_w	Sludge extraction flow rate ($L{\cdot}h^{-1}$)
r_{dCOD}	COD degradation rate, expressed in ($gCOD{\cdot}L^{-1}{\cdot}h^{-1}$)
r_{pCH_4}	Methane production rate, expressed in ($L\text{-}CH_4{\cdot}L^{-1}{\cdot}h^{-1}$)
R_0	Membrane intrinsic resistance (m^{-1})
R_c	Cake layer resistance (m^{-1})
$R_{F/BW}$	Filtration-cleaning ratio (−)
R_p	Pore blocking resistance (m^{-1})
R_t	Total resistance (m^{-1})
SMP	Soluble Microbial Products
S_p	Pore blocking mass (g)
S_{1in}	Inlet organic matter concentration ($g{\cdot}L^{-1}$)
S_{2in}	Inlet volatile fatty acids concentration ($g{\cdot}L^{-1}$)
SEC_P	Specific Energy Consumption of the Permeate pump ($Wh{\cdot}m^{-3}$)
t^{OC}_{BW}	Backwashing time for optimal control (s)
t^{TM}_{BW}	Backwashing time for temporized mode (s)
t^{OC}_{PC}	Physical cleaning time for optimal control (s)
t^{TM}_{PC}	Physical cleaning time for temporized mode (s)
T_{cyc}	Filtration/Backwash cycle duration (min)
TMP	TransMembrane Pressure (Pa)
u	Control variable =(1 or −1)
$\overline{u}$	Optimal control variable = [-1 1]
V	Reactor volume (L)
VFA	Volatile Fatty Acids
X_1	Acidogens concentration ($g{\cdot}L^{-1}$)
X_2	Methanogens concentration ($g{\cdot}L^{-1}$)
y_i	Experimental values
$\bar{y}_i$	Mean of the experimental values
$\hat{y}_i$	Model-predicted values
α	Specific cake-layer resistance ($m{\cdot}g^{-1}$)
α'	Specific pore blocking resistance ($m{\cdot}g^{-1}$)
β	Fraction of SMP blocking the pores (−)
ϵ	Porous surface fraction (−)
Δ_{sat}	Saturation degree (−)
γ	Fraction of S_T blocking the pores (−)
σ	Fictive cake layer mass (g)
σ'	Fictive pore blocking mass (g)
μ	The permeate viscosity (Pa·s)
μ_{max1}	Maximum acidogenic biomass growth rate on S_1 (h^{-1})
μ_{max2}	Maximum methanogenic biomass growth rate on S_2 (h^{-1})
μ_{SMPmax}	Maximum acidogenic biomass growth rate on SMP (h^{-1})
τ_{pCH_4}	Methane yield, defined as the volume of methane produced per gram of COD removed ($L\text{-}CH_4{\cdot}gCOD^{-1}_{removed}$)
ω	Detachment rate of reversible fouling (h^{-1})
ω'	Detachment rate of internal fouling (h^{-1})

1. Introduction

Controlling energy consumption has become a major challenge in the operation of membrane-based treatment systems (Maaz et al., 2019). In this context, anaerobic membrane bioreactors (AnMBRs) have emerged as a promising alternative for domestic wastewater treatment (DWWT), combining the benefits of anaerobic digestion, such as low sludge production and energy recovery through biogas, with the effective solid–liquid separation offered by membranes (Das et al., 2022; Gao et al., 2025; Mannina et al., 2021). However, the performance of these systems can be severely compromised by membrane fouling phenomena, biomass washout, and a biological dynamic (Abuabdou et al., 2020).

Membrane bioreactors (MBRs) incur notable energy demands, primarily associated with permeate pumping, sustaining membrane flux, and, specifically for aerobic systems, the energy-intensive aeration required for biological activity. Modeling studies report that the total energy consumption of aerobic MBRs is around 2 $kWh{\cdot}m^{-3}$ for municipal wastewater (~0.4 g $COD{\cdot}L^{-1}$), largely driven by aeration (Gao et al., 2025; Martin et al., 2011). AnMBRs, although they eliminate aeration, still require energy for filtration, with reported consumptions ranging from 0.27 to 0.45 $kWh{\cdot}m^{-3}$ for submerged systems, while side-stream units can be more demanding due to higher cross-flow velocities (Lei et al., 2018; Seib et al., 2016; Uman et al., 2021; Zielińska and Ojo,

2023). Fouling control, mainly through biogas sparging, accounts for 0.08–0.35 kWh·m^{-3} (up to 70–86% of the total demand) and can increase overall consumption to 16 kWh·m^{-3} under constrained side-stream conditions (Li et al., 2023; Tomczak et al., 2023; Zielińska and Ojo, 2023). However, AnMBRs stand out from aerobic systems thanks to methane produced from the organic matter in wastewater, which can be valorized on-site, offsetting part or even all of the treatment energy demand (Jiménez-Benítez et al., 2023). Depending on operational conditions (e.g., OLR and dissolved methane recovery), the recoverable methane energy typically ranges from 0.15 to 0.7 kWh·m^{-3} (Kong et al., 2021; Lei et al., 2018; Sanchez et al., 2022; Vinardell et al., 2020). This recovery can substantially offset overall energy demand, reinforcing the potential of AnMBRs for sustainable wastewater treatment and the need for integrated modeling to optimize their operation.

In this context, integrated modeling has become essential for understanding and optimizing AnMBR systems (Robles et al., 2018). While adapted activated sludge models such as ADM1 are parameter-intensive and poorly suited to explicitly incorporate membrane fouling (Batstone et al., 2002), simplified dynamic models such as the AM2/AM2b (Benyahia et al., 2024), provide effective descriptions of anaerobic digestion and methane production, including soluble microbial products (SMP). These models have proven effective in reliably describing organic matter degradation and methane production. On the physical side, various fouling models have been developed to represent pore blocking and cake formation and are often coupled with hydraulic or energy models (Chaaben et al., 2025; Gao et al., 2022; Jang et al., 2024). Recent studies have sought to integrate these biological and physical aspects into unified models to better capture the complexity of MBR systems (González et al., 2018; Mannina et al., 2021).

However, most existing models overlook a critical phenomenon in AnMBRs: the remobilization of biomass and substrates attached to the membrane during backwashing or relaxation phases. Neglecting this leads to mass imbalance, especially in low-load systems where attached biomass may represent a significant fraction of the active biomass. Moreover, the attachment/detachment dynamics of biomass and its typically lower biological activity in the biofilm strongly affect treatment performance and energy production (Jo et al., 2016; L. Smith et al., 2015). Additionally, introducing granular sludge into AnMBRs (G-AnMBRs) further enhances biomass retention, methane production, and process stability. Dense microbial aggregates promote sedimentation and reduce sensitivity to hydraulic variations (González et al., 2018). The intrinsic complexity of the system, arising from physico-chemical interactions and cyclic filtration operations, makes its behavior difficult to predict without rigorous modeling tools. Accordingly, several studies have used coupled models to assess the impact of backwash frequency on TMP and identify energetically optimal operating cycles. On the other hand, Ho and Sung (2010) demonstrated that microbial activity in biofilms is significantly lower than in suspended sludge (Ho and Sung, 2010); more recent works have further shown that biofilm-associated and suspended biomass exhibit distinct microbial community dynamics and functional limitations due to mass transfer constraints in MBRs (Harb et al., 2015; Kim et al., 2023; Sohn et al., 2024). This justifies the need to optimize filtration cycles to limit the growth of a low-activity biofilm.

Against this backdrop, the present study proposes an enhanced coupled modeling framework extending previous AM2b-based AnMBR approaches. The model integrates AM2b with a two-resistance fouling model (cake formation and pore blocking) and explicitly accounts for the return of detached material during physical cleaning, ensuring mass balance closure and capturing the impact of fouling-layer biomass on biological activity. The model is identified and validated using experimental data from a continuously operated G-AnMBR pilot. The proposed framework explicitly captures the coupled effects of fouling, backwashing, and biomass immobilization on methane production and net energy balance (NEB), an aspect that has not been addressed in existing AM2b-based AnMBR models. In particular, the influence of filtration/backwash cycle duration on energy recovery is systematically analyzed. As such, the proposed coupled model offers a systemic analytical framework to explore trade-offs between treatment efficiency, fouling control, and energy recovery, and constitutes a valuable basis for energy-oriented optimization and control of G-AnMBR systems.

2. Materials and methods

2.1. Experimental set-up

The entire experimental setup was designed and manufactured in the mechanical workshop of the European Membrane Institute (Montpellier, France). The biological reactor is a sealed opaque PVC tank, with internal dimensions of 266 mm (length) × 68 mm (width) × 523 mm (height). The reactor had a liquid working volume of 6.2 L and a gas headspace of 2.2 L. The pilot operation is controlled by a Programmable Logic Controller (PLC) designed by AC2I Automation (France). A flat polyethersulfone (PES) membrane (Microdyn-Nadir®, Germany) with a pore size of 0.04 μm and a filtration surface area of 0.34 m^2 is immersed at the center of the G-AnMBR reactor. The membrane module consists of three sheets (25 × 25 cm), with 5 mm spacing between them, and in center is a hole with diameter about 8.6 cm. Permeate suction from the center of the membrane is achieved using a peristaltic pump controlled by the PLC. An intermittent filtration cycle was applied, comprising 8 min 15 s of filtration(F), 30 s of relaxation(R), 45 s of backwashing (BW), and another 30 s of relaxation(R), as the only direct actuator to limit membrane fouling (No gas sparging). The backwash flux was set at 15 LMH. The backwash water is drawn from the treated wastewater storage tank. Continuous recirculation from the top to the bottom of the reactor was used to provide an Upflow Liquid Velocity (ULV) of 2.6 m·h^{-1} (Table 1 and Appendix A).

The G-AnMBR consisted of a single integrated unit combining an anaerobic bioreactor and a submerged membrane module. The reactor configuration and inoculation strategy have been previously described in detail in (Sanchez et al., 2023), and are only briefly summarized here. The system was inoculated with granular sludge obtained from a mesophilic (35–38 °C) Upflow Anaerobic Sludge Blanket reactor treating wastewater from a recycled paper factory operating at an OLR of 18 kgCOD·m^{-3}·d^{-1}. This sludge was gradually acclimatized over 20 months to low-strength wastewater (0.5 kgCOD·m^{-3}·d^{-1}), under hydraulic retention time (HRT) ranging from 10 to 30 h, achieving COD removal efficiencies of 80% ±15%, and at 25 °C, prior to the start of the present study. The total solids concentration in the G-AnMBR was maintained between 70 and 80 gTS·L^{-1}. No sludge was extracted throughout the experimental period, except for periodic sampling.

A complex synthetic influent was prepared to simulate domestic wastewater, following the protocol described in previous studies (Layer et al., 2019). The feed solution was renewed weekly and stored at 4 °C for up to one week. On average, the influent composition during the experimental period was approximately 290–350 mgCOD·L^{-1} for total COD (tCOD), 250–290 mgCOD·L^{-1} for soluble COD (sCOD), 40–60 mgCOD·L^{-1} for particulate COD (pCOD), and 160–210 mgCOD·L^{-1} for volatile fatty acids (VFA).

Table 1
Operation conditions of AnMBR.

Parameter	Unit	Value
Operating	d	50
Jp_{20net}	LMH	3.6 ± 1.4
HRT	h	4.9 ± 1.2
OLR	kgCOD·m^{-3}·d^{-1}	1.6 ± 0.7
Temperature	°C	25.2 ± 2.0
pH	–	7.4 ± 0.2
Redox	mV	−478 ± 23
ULV	m·h^{-1}	2.60 ± 0.03

2.2. Analytical methods

Influent, supernatant, and effluent samples were collected to measure total and soluble COD concentrations using commercial kits (Hach, Germany; LCK 500, 314, 514). Soluble COD concentration was then determined after pre-filtration of the samples through a 0.45 µm membrane filter. The supernatant was sampled from the top of the biological tank. The difference in soluble COD between the influent and the supernatant was attributed to biological removal, while the difference between the supernatant and the permeate was attributed to membrane removal (Biofilm and membrane cut-off). Volatile fatty acids (VFAs) were regularly analyzed using ion exclusion chromatography (ICS-900, Dionex, USA; BP-OA_2000 column, Benson Polymeric Inc., USA) coupled with a UV detector at 210 nm. H_2SO_4 (0.05 N) was used as the eluent at a flow rate of 0.4 mL·min^{-1}. All samples were filtered through a 0.22 µm membrane prior to HPLC-UV analysis. Total and volatile suspended solids (TSS and VSS) in the mixed liquor were measured according to Standard Methods (Lipps et al., 2023).

Produced methane was measured in the gas and liquid phases. The gas-phase flow rate was continuously monitored using a volumetric flow meter (MilliGas Counter, Ritter, Germany). The methane (CH_4) and carbon dioxide (CO_2) contents, in gas phase, were quantified using a gas chromatograph (GC 7890B, Agilent Technologies, USA) equipped with a thermal conductivity detector (TCD) and a stainless-steel packed column (Porapak Q, 2 m × 3 mm) (Sanchez et al., 2022). The dissolved methane (CH_4^L (mg·L^{-1})) was quantified experimentally following the headspace method described by (Giménez et al., 2012; Sanchez et al., 2022).

The saturation degree (Δ_{sat}) was calculated based on the theoretical value of methane dissolved in the liquid phase ($C^L_{CH_4}$) calculated according to the Henry's law thermodynamic in equilibrium with the gas phase as described in Eq. (1)

$$\Delta_{sat} = \frac{C^L_{CH_4}}{H(T)\cdot C^G_{CH_4}} \quad (1)$$

Where $C^G_{CH_4}$ is the methane concentration in the gas phase (mg·L^{-1}) and H(T) is the dimensionless temperature-dependent Henry's constant for methane (Giménez et al., 2012).

2.3. Process modelling

Coupled (or integrated) models take into account the two main operations of the MBR process: biological treatment ("biomass kinetics") and physical treatment ("membrane filtration") (Fig. 1) (Hamedi et al., 2021; Mannina et al., 2021). These coupled models are essential to link the impacts between biological processes and the separation step.

2.3.1. Anaerobic biological kinetics

The biological dynamics follow the AM2b model proposed by Benyahia et al., (2024), developed for AnMBR systems which assumes that the biological system is reduced to two microbial populations: acidogenic bacteria (X_1) and methanogenic bacteria (X_2). Then, acidogenic bacteria (X_1) convert organic matter (S_1) into volatile fatty acids (S_2), which are then consumed by methanogenic bacteria (X_2) to produce methane (Table 2). The growth and decay of both populations generate SMP, composed mainly of proteins and polysaccharides, which are key contributors to membrane fouling mechanisms such as pore blocking and gel layer formation (Drews, 2010; Guo et al., 2022).

Taking into account the biological reactions and assumptions described above, the concentration dynamics of X_1, X_2, S_1, S_2 and SMP linked to biological activity in the bioreactor can be described in equations (2), (3), (4), (5) and (6), respectively.

$$f_{X_1}(X_1, S_1, SMP) = (\mu_1 + \mu_{SMP} - k_{d1})\cdot X_1 \quad (2)$$

$$f_{X_2}(X_2, S_2) = (\mu_2 - k_{d2})\cdot X_2 \quad (3)$$

$$f_{S_1}(X_1, S_1) = -k_1\cdot\mu_1\cdot X_1 \quad (4)$$

$$f_{S_2}(X_1, X_2, S_1, S_2, SMP) = -k_3\cdot\mu_2\cdot X_2 + (k_2\cdot\mu_1 + b_2\cdot\mu_{SMP})\cdot X_1 \quad (5)$$

$$f_{SMP}(X_1, X_2, S_1, S_2, SMP) = (b_3\cdot\mu_1 + k_{d1} - b_1\cdot\mu_{SMP})\cdot X_1 + (b_4\cdot\mu_2 + k_{d2})\cdot X_2 \quad (6)$$

As demonstrated in the literature about ADM1 and AM2 model (Batstone et al., 2002; Bernard et al., 2001), the growth kinetic μ_1 of acidogens (X_1) by consuming COD (S_1) and the growth kinetic μ_{SMP} of acidogens (X_1) by consuming SMP expressed in Eqs. (7) and (9) respectively, are based on Monod function. However, the growth kinetic μ_2 of methanogens (X_2) by consuming VFA (S_2) expressed in Eq. (8) is based on the Haldane function considering the inhibition effect on acidogens growth with a high VFA concentration.

$$\mu_1(S_1) = \mu_{1max}\cdot\frac{S_1}{K_1 + S_1} \quad (7)$$

$$\mu_2(S_2) = \mu_{1max}\cdot\frac{S_2}{K_2 + S_2 + \frac{S_2^2}{K_i}} \quad (8)$$

$$\mu_{SMP} = \mu_{SMPmax}\cdot\frac{SMP}{K_3 + SMP} \quad (9)$$

2.3.2. Coupled model with membrane dynamics (coupling the model with the membrane step)

The contribution of soluble components ("$S_T = S_1 + S_2$" and "SMP") and particulate components ("$X_T = X_1 + X_2$") to the formation of the cake layer $m_c(t)$ depends on the reactor hydrodynamics, through the

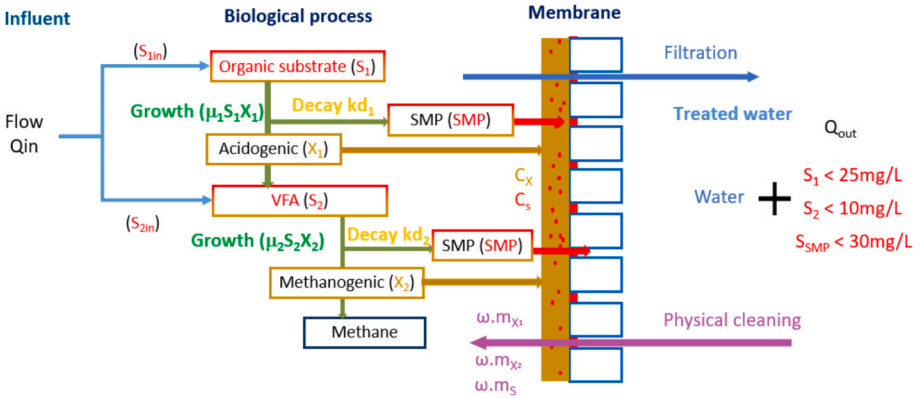

Fig. 1. Coupled model modified AM2b for G-AnMBR.

Table 2
AM2b model reactions.

Acidogenesis and SMP production: $k_1 S_1 \rightarrow X_1 + k_2 S_2 + b_3 SMP + k_4 CO_2$
Methanogenesis and SMP production: $k_3 S_2 \rightarrow X_2 + b_4 SMP + k_5 CO_2 + k_6 CH_4$
SMP degradation: $b_1 SMP \rightarrow X_1 + b_2 S_2 + k_7 CO_2$
SMP production from biomass decay: $k_{d1} X_1 \rightarrow k_{d1} SMP$, $k_{d2} X_2 \rightarrow k_{d2} SMP$

attachment coefficients C_s for soluble components and C_x for particulate components. Based on previous studies (Benyahia et al., 2024; Sanchez et al., 2023), the attachment coefficient for soluble products (C_s) is consistently much lower than that for particulate matter (C_x). Additionally, the contribution of substrates "S_T" and "SMP" to pore constriction $S_p(t)$ with fractions γ and β, respectively, was also considered. Both components, $m_c(t)$ and $S_p(t)$, have their own dynamics: they increase during the filtration phase and decrease during the backwashing/relaxation phases. Instead of adopting Benyahia's assumption that the material attached to the membrane is negligible compared to that present in the reactor (an assumption that could lead to biomass washout due to the loss of these materials from the mass balance), this model has been upgraded by accounting for the impact of sludge entrapped on the membrane, as well as the contribution of material detached during backwash to the bulk suspension. The mass of the cake layer was also divided according to its composition into particulate components ($m_{x1}(X_1)$ and $m_{x2}(X_2)$) and soluble components (m_s (S_1, S_2, SMP)). By convention, a control variable u = 1 is assumed during the filtration phase and u = –1 during the physical cleaning phase. The dynamics of the mass $m_c(t)$ and $S_p(t)$ during filtration and physical cleaning phases were proposed as shown in equations (10–14):

$$\dot{m}_{X1} = \frac{1+u}{2}(Q_{out} \cdot C_{X1} \cdot X_1) - \frac{1-u}{2}(\omega \cdot m_{X1}) \tag{10}$$

$$\dot{m}_{X2} = \frac{1+u}{2}(Q_{out} \cdot C_{X2} \cdot X_2) - \frac{1-u}{2}(\omega \cdot m_{X2}) \tag{11}$$

$$\dot{m}_S = \frac{1+u}{2} \cdot Q_{out} \cdot \left(\sum C_{Si} \cdot S_i + C_{SMP} \cdot SMP \right) - \frac{1-u}{2}(\omega \cdot m_s) \tag{12}$$

$$m_c = m_{X1} + m_{X2} + m_S \tag{13}$$

$$\dot{S}_p = \frac{1+u}{2} \cdot (Q_{out} \cdot (\beta \cdot SMP + \gamma \cdot S_T)) - \frac{1-u}{2} \cdot (\omega' \cdot S_p) \tag{14}$$

To avoid unnecessarily complicating the model, the amount of soluble products detached during the physical cleaning phase was considered negligible relative to the amount present in the influent (equations (16–18)). Under these assumptions, the reinjection of detached material into the mass balance accounts only for the particulate fractions (equations (15) and (16)).

$$\dot{X}_1 = f_{X_1}(X_1, S_1, SMP) - \frac{1+u}{2}\left(\frac{Q_{out}}{V} \cdot C_{x1} + \frac{Q_w}{V}\right) X_1 + \frac{1-u}{2}\left(\frac{\omega \cdot m_{X1}}{V} - \frac{Q_w}{V} \cdot X_1\right) \tag{15}$$

$$\dot{X}_2 = f_{X_2}(X_2, S_2) - \frac{1+u}{2}\left(\frac{Q_{out}}{V} \cdot C_{x2} + \frac{Q_w}{V}\right) X_2 + \frac{1-u}{2}\left(\frac{\omega \cdot m_{X2}}{V} - \frac{Q_w}{V} \cdot X_2\right) \tag{16}$$

$$\dot{S}_1 = f_{S_1}(X_1, S_1) + \frac{1+u}{2}\left(\frac{Q_{in}}{V} \cdot S_{1in} - \Psi_{S1} \cdot S_1\right) - \frac{1-u}{2}\left(\frac{Q_w}{V} \cdot S_1\right) \tag{17}$$

$$\dot{S}_2 = f_{S_2}(X_1, X_2, S_1, S_2, SMP) + \frac{1+u}{2}\left(\frac{Q_{in}}{V} \cdot S_{2in} - \Psi_{S2} \cdot S_2\right) - \frac{1-u}{2}\left(\frac{Q_w}{V} \cdot S_2\right) \tag{18}$$

$$\dot{SMP} = f_{SMP}(X_1, X_2, S_1, S_2, SMP) + \frac{1+u}{2}(-\Psi_{SMP} \cdot SMP) - \frac{1-u}{2}\left(\frac{Q_w}{V} \cdot SMP\right) \tag{19}$$

$$\Psi_{Si} = \frac{Q_{out}}{V}(1 - (C_{si} + \gamma)) + \frac{Q_w}{V} \text{ and } \Psi_{SMP} = \frac{Q_{out}}{V}(1 - (C_{SMP} + \beta)) + \frac{Q_w}{V} \tag{20}$$

2.3.3. Constant flux model: Series resistance model

The AM2b model is coupled with a two-parameter fouling model that accounts for cake layer fouling and pore blocking (Benyahia et al., 2024; Sanchis-Perucho et al., 2024): i) The first mechanism is caused by the mass $m_c(t)$ of particular compounds that accumulate on the membrane surface, also referred to as cake layer formation or cake fouling, and ii) The second mechanism is due to colloidal or soluble compounds $S_p(t)$ retained within the membrane pores in the form of SMP and substrates S_1 and S_2, referred to here as pore constriction. Their concentrations are not assumed constant but are dynamically simulated based on biological activity. These compounds can be smaller than the pore size and are known to progressively clog the membrane pores.

The proposed modeling approach, grounded in the series resistance concept, enables a dynamic decoupling of the different fouling mechanisms (solids accumulating on the membrane surface vs. SMP-induced pore blocking). According to this framework derived from Darcy's law, the membrane fouling model for systems operating at a constant permeate flux (J_P) is expressed by equation (21).

$$TMP = J_p \cdot \mu \left(R_0 + R_c(m_c(t)) + R_p(S_p(t)) \right) \tag{21}$$

J_P: Permeate flux (LMH), TMP: Transmembrane pressure (Pa), μ: dynamic viscosity (Pa.s), R_0: intrinsic membrane resistance (m^{-1}), R_c: cake layer resistance (m^{-1}), and R_p: pore blocking resistance (m^{-1}). The total resistance (R_t) accounts for both cake formation and pore blocking.

The resistances R_c and R_p depend on the mass $m_c(t)$ and the concentration $S_p(t)$, respectively, as well as on the filtration surface area.

$$R_c(m_c(t)) = \alpha\left(\frac{m_c(t)}{A(t)}\right), \quad R_p(S_p(t)) = \alpha'\left(\frac{S_p(t)}{\epsilon A(t)}\right) \tag{22}$$

α: specific cake resistance ($m \cdot g^{-1}$), α': specific resistance of pore blocking ($m \cdot g^{-1}$), $A(t)$: dynamic of filter surface (m^2), and ∈: initial membrane porosity.

The effective filtration surface area of the membrane is assumed to vary during operation, and is described in equation (23):

$$A(t) = \frac{A_0}{1 + \frac{m_c(t)}{\sigma} + \frac{S_p(t)}{\sigma'}} \tag{23}$$

A_0: initial membrane surface (m^2), σ and σ': half-saturation cake layer and pore blocking mass, respectively, of the effective filtration surface (g).

The parameters σ and σ′ represent characteristic half-saturation masses of the effective filtration surface, i.e., the amounts of cake layer or pore-blocking foulants required to reduce the effective membrane area by 50% when acting alone.

However, in practice, after each backwashing or relaxation cycle, a certain quantity of $m_c(t)$ and $S_p(t)$ remain attached, progressively contributing to irreversible fouling. Over time, the effective surface area A(t) gradually decreases, resulting in a sustained degradation of membrane performance.

2.3.4. Biogas production

2.3.4.1. Modelling of methane production. The biogas produced during the biological process, according to the reactions in Table 2, consists of carbon dioxide (CO_2) and methane (CH_4). The key advantage of anaerobic digestion lies in the generation of methane, which can be considered an energy source to offset the energy demand of this treatment process. The high methane content is beneficial for the energy balance and indicates good performance of the methanogenic microbial populations (Chen et al., 2020).

In this model, only methane (CH_4) production is considered, as it represents the energetically valuable fraction of the biogas. Methane is produced in a single step during the methanogenesis (Table 2) and is described following the approach of Bernard et al., (2001) (Equations (24)–(26)). The methane production rate is assumed to be equal to the biogas production rate, as transient effects in the liquid phase can be neglected under the constant OLR used in this study.

$$r_{pCH_4} = k_6 \cdot \mu_2 \cdot X_2 \tag{24}$$

$$r_{dCOD} = ((k_1 - k_2)\cdot\mu_2 + k_2\cdot\mu_{SMP})X_2 + (k_3 - b_4)\mu_2\cdot X_2 \tag{25}$$

$$\tau_{pCH_4} = \frac{r_{pCH_4}}{r_{dCOD}} \tag{26}$$

r_{pCH_4}: Methane production rate, expressed in L-CH_4·L^{-1}·h^{-1}, r_{dCOD}: COD degradation rate, expressed in gCOD·L^{-1}·h^{-1}, τ_{pCH_4}: Methane yield, defined as the volume of methane produced per gram of COD removed, expressed in L-CH_4·$gCOD_{removed}^{-1}$, and k_6: Yield coefficient for methane production, expressed in L-CH_4·$gCOD^{-1}$.

2.3.4.2. Experimental determination of methane production. Table 3 reports the key outcomes measured at an OLR of 1.6 ± 0.7 kgCOD·m^{-3}·d^{-1} (Sanchez et al., 2022). The methane gas flow reached 2.42 ± 0.20 NL-CH_4·d^{-1} at steady state. The dissolved methane concentration was 12.8 mg-CH_4·L^{-1}, representing about 14.3% of the total methane produced. In the methane mass balance, the total methane production rate is therefore computed as the sum of the gas-phase flow and the dissolved methane leaving with the liquid effluent. The total methane yield was 0.31 ± 0.03 NL-CH_4·$gCOD_{removed}^{-1}$.

3. Results and discussion

3.1. Modified-AM2b identification

The modeling of experimental data from the G-AnMBR was carried out based on the study campaign operated at permeate flux of 6.0 ± 1.4 LMH (Appendix A), while the campaign, operated at a flux of 4.1 ± 1.2 LMH, is used to validate the model. For the identification, data collected over a period of approximately 50 days were simulated using the modified AM2b model described in Section 2.3. An experimental validation approach was implemented to assess the agreement between the model-generated results and the experimental measurements. In other words, the model was compared to experimental data to best calibrate the system outputs. Parameter identification was performed in MATLAB R2020a using the fmincon algorithm with a constrained least-squares objective function (Eq. (27)), in order to optimize the attachment coefficient (C_x, C_s) and the backwash efficiency (w and w′). Model performance was assessed through the coefficient of determination (R^2) (Eq. (28)).

$$LS = \sum (y_i - \hat{y}_i)^2 \tag{27}$$

$$R^2 = 1 - \sum_{i=1}^{n} \frac{(\hat{y}_i - \bar{y}_i)^2}{(y_i - \bar{y}_i)^2} \tag{28}$$

$\hat{y}_i$: Model-predicted values, y_i: Experimental values, and $\bar{y}_i$: Mean of the experimental values.

Default biological parameters were taken from previous studies (Benyahia et al., 2024; Bernard et al., 2001), whereas a limited number of biological parameters and all fouling-related parameters were estimated in this study using experimental data, and are presented in Table 4.

To calibrate the biological model against the experimental data, the selection of the parameters to be estimated was determined by the measurements available in the dataset. The estimated biological parameters listed in Table 4 were identified using the least squares (LS) method in order to accurately reproduce the observed biological dynamics, namely the variations of the outlet substrates (S_1, S_2, SMP) and the methane (CH_4) production.

As a synthetic influent was used, SMP concentrations at the reactor inlet were assumed to be zero. SMP were therefore generated exclusively by biological activity through biomass growth and decay processes. A fraction of SMP was assumed to contribute to membrane fouling pore blocking, based on experimental fouling layer characterization (Sanchez et al., 2023).

During this campaign, substrates (S_1 and S_2) and SMP and complementary analyses under various flux and OLR conditions showed concentrations ranging from 13 to 50 mg·L^{-1}. Integrating the reintegration of detached biomass into the model proved essential, as it markedly improved the consistency of the predicted profiles. With this modification, the identified model successfully reproduced the observed substrate trends as SMP, achieving an R^2 of 0.88 (Fig. 2), and providing more accurate predictions than the original formulation.

The results indicate that substrate degradation proceeded rapidly, with S_1 and S_2 approaching steady-state conditions as early as day 6 (Ramakrishnan and Surampalli, 2012; Duong et al., 2020; Sanchez et al., 2022). In contrast, SMP responded more slowly and only stabilized after approximately 10 days, reflecting their continuous production during both acidogenic and methanogenic stages, as well as their release through microbial decay. In addition to soluble substrates, biomass accumulation in the bioreactor was assessed through VSS measurements at the end of the experimental period. The VSS concentration was measured at approximately 71.1 ± 4.3 gVSS·L^{-1}. The accumulation of VSS observed at the end of operation corresponds to an apparent biomass yield of about 0.1 gVSS·$gCOD_{removed}^{-1}$, highlighting the low sludge yield characteristic of G-AnMBRs (Sanchez et al., 2022).

The filtration-related parameters were estimated (Table 4) by fitting the model outputs to the experimental system data (TMP) using the least squares method. The attachment coefficients (C_X, C_S, and C_{SMP}) are the fractions of biomass and substrates that attach to the membrane, which is defined as being between 0 and 1. The physical cleaning efficiencies w and w' are expressed in terms of frequency, i.e., their ability to detach attached material per unit of time must be positive. The specific cake resistance (α) is highly variable depending on particle size, porosity, and cake compressibility, with typical values in MBRs ranging from 1 x10^{11} to 1 x10^{14} m·kg^{-1} (Du et al., 2020).

Table 3
Methane production (liquid and gas).

	Unit	Value
Gaseous methane flow rate	NL-CH_4·d^{-1}	2.42 ± 0.20
Gaseous methane yield	NL-CH_4·$gCOD_{removed}^{-1}$	0.27 ± 0.03
Dissolved methane concentration	mgCH_4·L^{-1}	12.8 ± 0.7
Dissolved methane flow rate	NL-CH_4·d^{-1}	0.35 ± 0.03
Saturation degree (Δ_{sat}) (Eq. (1))	–	2.0 ± 0.1
Total methane yield	NL-CH_4·$gCOD_{removed}^{-1}$	0.31 ± 0.03

3.2. Membrane fouling

The developed model simulates both reversible and irreversible fouling, represented respectively by the mass of the cake layer deposited

Table 4
Default biological parameters from literature sources (Benyahia et al., 2024; Bernard et al., 2001), and estimated biological and fouling parameters obtained using LS method.

	Parameter	Value	Parameter	Value	Parameter	Value
Default biological parameters	b_1 (−)	1	K_1 ($g{\cdot}L^{-1}$)	0.71	μ_{max1} (h^{-1})	1.2
	b_2 (−)	0.5	K_2 ($g{\cdot}L^{-1}$)	0.14	μ_{max2} (h^{-1})	0.48
	b_3 (−)	2.5	K_3 ($g{\cdot}L^{-1}$)	0.6	μ_{SMPmax} (d^{-1})	1.2
	b_4 (−)	0.095	K_i ($g{\cdot}L^{-1}$)	15	$k_{d1} = k_{d2}$ (h^{-1})	5×10^{-4}
Estimated biological parameters	k_1 (−)	2	k_2 (−)	1.5	k_3 (−)	2.6
	β(−)	0.52	γ (−)	0.25	k_6 ($NL\text{-}CH_4{\cdot}gCOD^{-1}$)	0.826
Estimated fouling Parameters	C_X (−)	0.097	C_S, C_{SMP} (−)	2.25×10^{-3}	ω(h^{-1})	2.05
	ω′(h^{-1})	3.76×10^{-5}	α($m{\cdot}g^{-1}$)	6.3×10^{11}	α′($m{\cdot}g^{-1}$)	1.0×10^{10}
	σ and σ′ (g)	12.5				

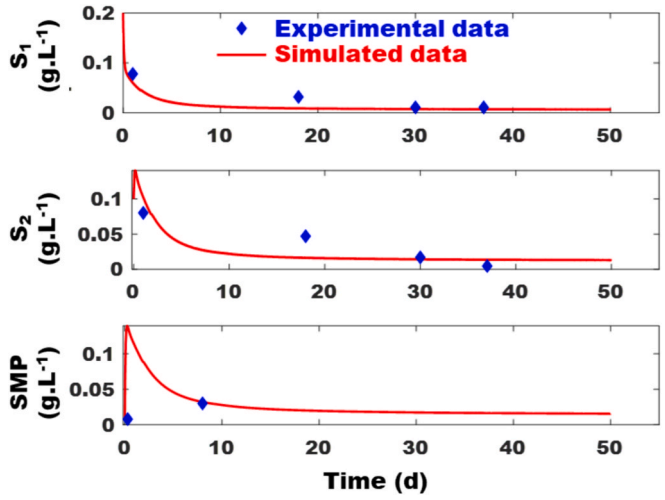

Fig. 2. Temporal variation of bulk substrate concentrations; *S_1, S_2 and SMP ($g{\cdot}L^{-1}$) in the G-AnMBR.*

on the membrane surface ($m_c(t)$) and the mass of particles obstructing the pores ($S_p(t)$). At the end of the G-AnMBR operation, the membrane was removed from the reactor to examine in detail the composition and reversibility of the fouling layer through a quantitative analysis (mass 'm_c') and a qualitative characterization (VSS, TSS, and SMP). This post-operation assessment was used to evaluate the accuracy of the model in reproducing the experimental TMP and to refine the fouling-related parameters.

As shown in Fig. 3(a), the simulation curve indicates that the identified model accurately reproduces the experimental TMP data over the full 50-day period, with a determination coefficient greater than 0.94. The TMP profile can be divided into two phases: a transient phase from the start of operation until day 9, during which fouling progressed rapidly (4.9 $kPa{\cdot}d^{-1}$), and a steady-state phase from day 9 onward, where TMP variation became negligible (~0 $kPa{\cdot}d^{-1}$). According to Fig. 3(c), the cake layer mass stabilized after 10 days at 45.1 ± 0.9 $g{\cdot}m^{-2}$. Under steady-state conditions, the mass of pore-blocking particles increased linearly, confirming its irreversible nature. Although particulate matter dominated the cake layer mass, the continued rise in pore-blocking resistance indicates that soluble and colloidal compounds, including SMP and residual substrates, mainly drove irreversible fouling. After 25 days, permeate flux declined, leading to a slight decrease in TMP; however, this reduction was not proportional due to the large membrane deposit and ongoing pore blocking.

To validate the identified model, parameters obtained from operation at flux of 6 ± 1.4 LMH were used to predict TMP variation during system operation at 4.1 ± 1.2 LMH and the model accurately reproduced the experimental data with an R^2 of 0.97 (Fig. 3(b)).

Table 5 summarizes the experimentally measured parameters available only at the end of the operation, their corresponding model-simulated values, and the relative errors between both sets of data. The relative errors between the model predictions and the experimental values range from 3.2% to 16.6%. This discrepancy may be attributed to the decline in permeate flux observed after day 25 of operation, which was not accounted directly by the model.

3.3. Methane production

The methane flow rate in the gas phase at steady state was 2.42 ± 0.20 $NL\text{-}CH_4{\cdot}d^{-1}$ when operating the reactor at an OLR of approximately 1.6 ± 0.7 $kgCOD{\cdot}m^{-3}{\cdot}d^{-1}$.

Fig. 4 shows the calibration of the model to the experimental methane production data, corresponding to the operating conditions presented in Table 1. A good agreement between the modified AM2b model and the experimental data was observed, with a determination coefficient of R^2 = 0,995. The optimal value identified for the methane yield parameter k_6 was 0.83 ± 0.05 $NL\text{-}CH_4{\cdot}gCOD^{-1}$.

The experimental steady state methane yield is around 0.314 $NL\text{-}CH_4{\cdot}gCOD^{-1}_{removed}$ with SD ± 0.030 and the model one is equal to 0.338 $NL\text{-}CH_4{\cdot}gCOD^{-1}_{removed}$. This difference may be due to the absence of disturbances in the model in contrast to experimental system which in front of different disturbances like temperature, pH, potential redox,… and error of measurements.

3.4. Effect of total period cycle on system performances

Fouling was controlled by periodically limiting the cake layer ($m_c(t)$ and $S_p(t)$) through backwashing and relaxation. Backwashing was applied by reversing the permeate flow to detach part of the cake and to dislodge pore-blocking particles, whereas relaxation was implemented by halting filtration to suppress convective deposition forces and promote back-diffusion, thereby partially disrupting the fouling layer. In this context, the influence of the cycle duration (T_{cyc} = filtration + physical cleaning) on the NEB, defined as the methane production (energy recovered) relative to the specific energy consumption of the permeate pump (SEC_p), was investigated. To isolate the effect of cycle duration, the filtration-to-backwashing ratio ($R_{F/BW}$) was kept constant. Since the actual dynamics of the deposited mass during the different physical cleaning steps are not well characterized experimentally, both mechanisms were assumed to have an equivalent effect during parameter identification and were therefore combined into a single physical cleaning phase.

To this end, a constant $R_{F/BW}$ was maintained across simulations, while the total cycle time was varied over a 50-day operational period. Model outputs show that longer T_{cyc} values lead to proportionally higher SEC_p (Fig. 5, Table 6) as the TMP is higher. This is attributed to increased accumulation and compression of fouling on the membrane, as longer filtration phases delay the initiation of cleaning. Consequently, TMP remains elevated for extended periods, intensifying energy demands. Moreover, the compressed fouling layer becomes more resistant to removal, further reducing the efficiency of physical cleaning (Poorasgari et al., 2015).

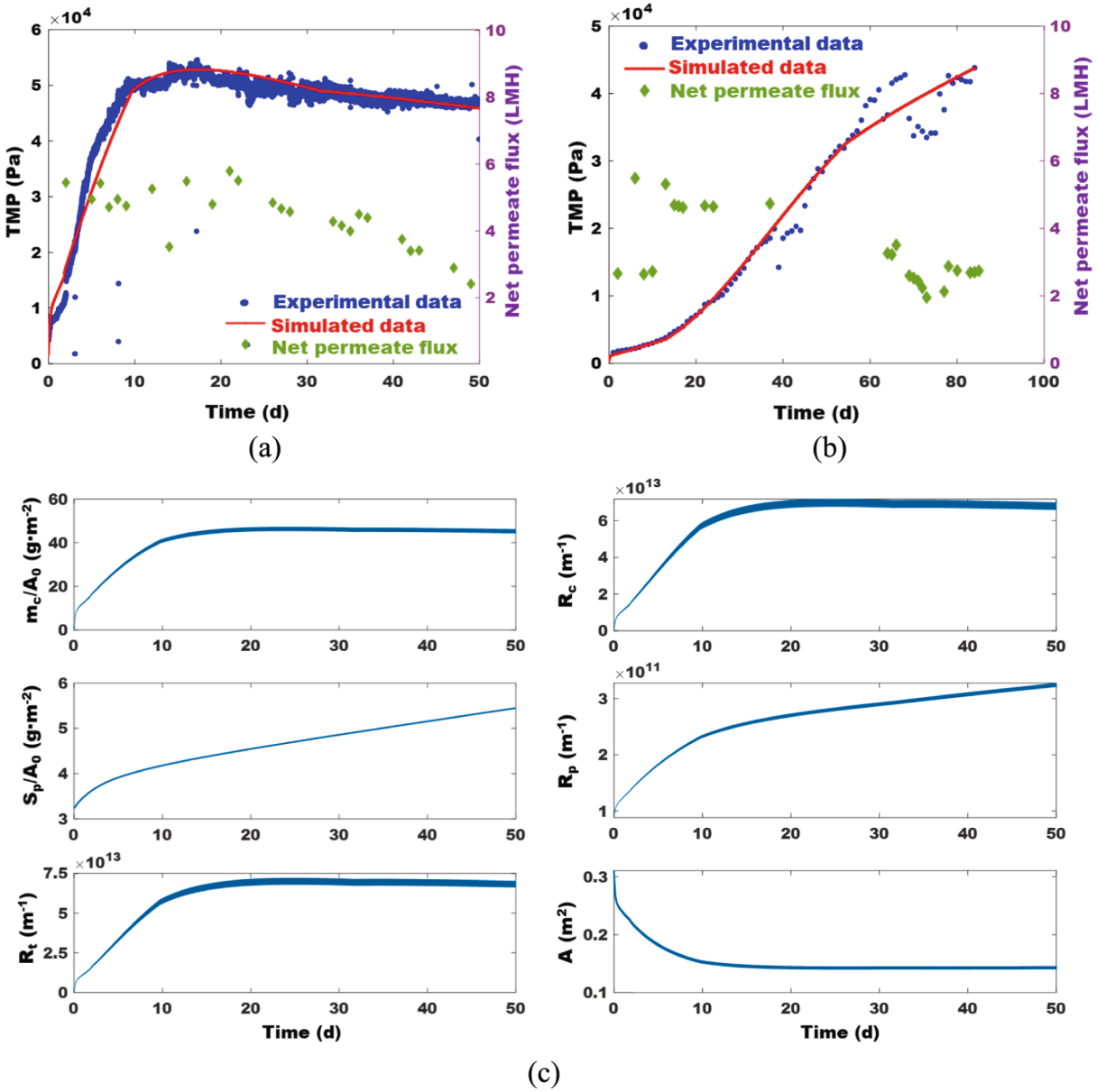

Fig. 3. (a): Simulated TMP fitted on experimental TMP and experimental net permeate flux variation during the calibration phase of the model, under an applied flux of 6 ± 1.4 LMH and HRT = 4.9 ± 1.2 h; (b): Model validation on TMP data and experimental net permeate flux variation during system operation at applied flux of 4.1 ± 1.2 LMH and at HRT = 7 ± 0.7 h, (c): simulated evolution cake layer mass (m_c) and resistance (R_c), pore blocking mass (S_p) and resistance (R_p), total resistance (R_t) and available membrane surface (A), obtained from the calibration results.

Table 5
Comparison of the experimental data with the simulated one when operation was terminated.

Parameter	Experimental value	Model value	Relative error (%)
m_c/A_0 (g·m^{-2})	45.9	44.4	3.2
R_c (m^{-1})	5.7 x 10^{13}	6.6 x 10^{13}	16.6
R_p (m^{-1})	3 x 10^{11}	3.2 x 10^{11}	7.0
R_{tot} (m^{-1})	5.7 x 10^{13}	6.6 x 10^{13}	16.5
A (m^2)	–	0.143	–

(–): Not Defined.

While maintaining a constant $R_{F/BW}$, variations in the overall T_{cyc} were found to significantly affect the methane production rate. Simulation results revealed that longer cycles lead to a reduction in methane yield. In the model, the fouling layer is assumed to consist of biologically inactive attached biomass. As the filtration phase is prolonged, a larger fraction of the active microorganisms becomes trapped and remains inactive for a longer period. Consequently, the effective biomass remaining in suspension to degrade organic substrates decreases. This effect is directly reflected in the mass balance: the concentration of active biomass available for conversion (X) governs the substrate degradation rate through the growth term μ·X. When a larger fraction of biomass becomes immobilized within the fouling layer, suspended biomass decreases, reducing the net biological conversion term in the substrate balance. Two factors reported in the literature support this modelling assumption: i) attached communities generally exhibit lower metabolic activity than suspended sludge (Cheng et al., 2019; Kim et al., 2023), and ii) substrate diffusion toward the membrane surface, as well as contact time, is limited in non-mixed systems (Harb et al., 2015), further restricting the activity of the attached biomass.

Based on the methane produced from COD conversion, the energy potentially recovered from DWWT was calculated. For the evaluation of

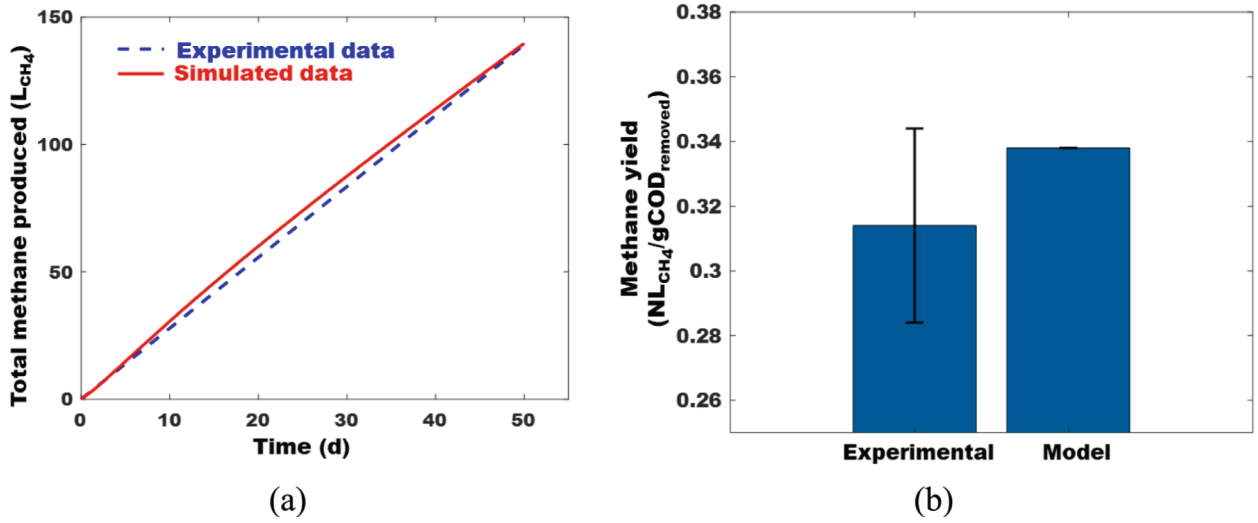

Fig. 4. Model adjustment on experimental methane production data during system operation under an applied filtration flux of 6 ± 1.4 LMH, corresponding to HRT = 4.9 ± 1.2 h; (a) Accumulated methane volume (NL-CH_4) over time, (b): Steady-state methane yield (NL-CH_4.$gCOD^{-1}$).

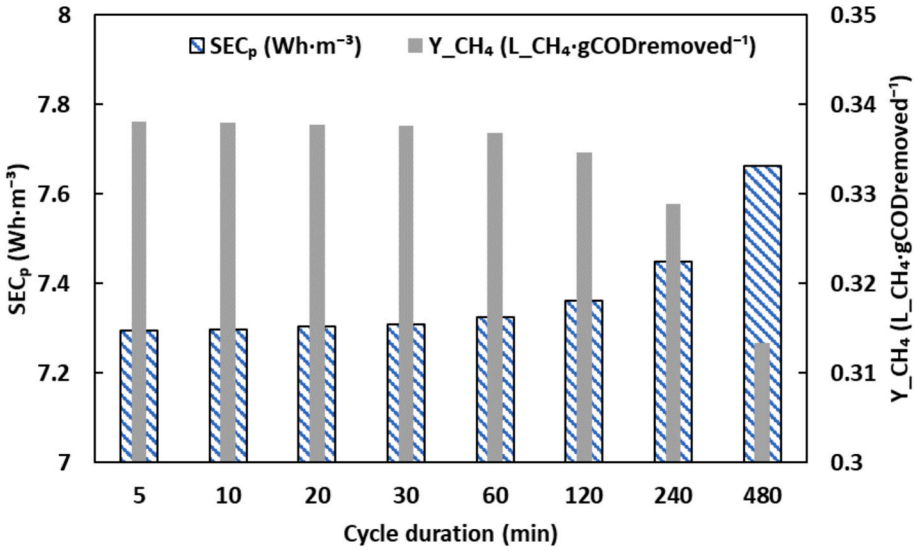

Fig. 5. Variation in specific energy consumption of permeate pump (SEC_P, kWh/m^3) and the specific methane production yield (Y_CH_4, $LCH_4{\cdot}gCOD^{-1}_{removed}$) as a function of the cycle duration.

Table 6
Energy balance over 50 days of system operation.

Cycle period (min)	System total energy required ($Wh{\cdot}m^{-3}$)	% of the energy consumption of permeate pump (%)	Recovered energy produced ($Wh{\cdot}m^{-3}$)	Total energy produced ($Wh{\cdot}m^{-3}$)	NEB ($Wh{\cdot}m^{-3}$)
5	120.0	6.1	618.7	721.9	498.7
10	120.0	6.1	618.5	721.7	498.5
20	120.0	6.1	618.1	721.3	498.0
30	120.0	6.1	617.7	720.8	497.5
60	120.0	6.1	616.3	719.1	495.7
120	120.1	6.1	612.4	714.6	491.3
240	120.2	6.2	601.7	702.1	479.6
480	120.2	6.4	573.4	669.1	450.2

the recoverable energy, only the gas-phase methane is considered, and the fraction leaving in the liquid (14.3%) is treated as an energetic loss. The energy balance in this study was calculated considering only methane recovered in the gas phase. This choice reflects current operational practice in AnMBR systems, where dissolved methane is generally not recovered without additional separation units. Any further improvement in energy performance would depend on the implementation and efficiency of dedicated dissolved methane recovery technologies (e.g., degassing units or membrane contactors), as well as on operating conditions such as temperature, which affects methane solubility. Based on the methane produced from COD conversion, the potential recoverable energy was estimated by converting the total

methane flow into its energy equivalent. Methane was transformed into energy using its lower heating value (LHV = 9.94 Wh·L-CH_4^{-1}), allowing direct calculation of the energy that can be theoretically recovered from the anaerobic digestion process (Dong et al., 2022; Shao et al., 2023). Table 6 provides an overview of the NEB variation and energy required for DWWT process at ambient temperature.

When operating with an AnMBR, the energy demand is partially offset by the methane produced, which enhances the value of this type of system thanks to a more favorable NEB. As shown in Fig. 5, the duration of the filtration/physical cleaning cycle influences both the SEC_p and the efficiency of methane recovery; however, the magnitude of these effects remains relatively limited under the operating conditions tested.

Table 6 summarizes the influence of the operating cycle duration on both energy consumption and energy recovery, and consequently, on the NEB of the system. The total energy consumption remains nearly constant across all tested cycle durations, with an average value of approximately 120 Wh·m^{-3}. In this context, the permeate pump accounts for only about 6.20% ± 0.16 of the overall energy demand, which is largely dominated by other components such as the recirculation pumps (≈ 30–40%) and temperature control at 25 °C (≈ 50–60%) (Martin et al., 2011; Sanchez et al., 2022). However, in other membrane filtration configurations –for instance, in inverted gravity systems or in the absence of thermal regulation and recirculation– the permeate pump may become the main or even the sole source of energy consumption. Under such conditions, changes in cycle duration result in only minor variations in NEB. Nevertheless, longer cycles progressively increase the energy required for permeation due to declining membrane permeability. Extending the cycle from 5 min to 8 h raises the SEC_p by about 5%. Consequently, the NEB decreases with increasing cycle duration: the highest NEB is obtained at T_{cyc} = 5 min, and extending the cycle to 30 min produces only a negligible loss (0.2%). A 2-hour cycle yields a more noticeable reduction (1%), while the most pronounced effect occurs at T_{cyc} = 8 h, where the NEB drops by nearly 9.7%. These results highlight that although gains remain modest in the present setup, excessively long filtration cycles can impose a clear energetic penalty when pump consumption becomes dominant.

3.5. Optimal control

In addition to experimental validation and the analysis of cycle duration on the NEB, an initial application of optimal control was conducted to demonstrate the model's potential for energy-oriented process management. The coupled model was used to optimize filtration/backwash cycles based on the formulation of Aichouche et al. (2020), which minimizes SEC_p under operational constraints using the Pontryagin Maximum Principle applied to a simplified filtration model (Appendix B).

Two operating regimes were considered: a transient phase (0–10 days), dominated by rapid cake accumulation, and a pseudo-steady-state phase (t > 10 days). For each regime, control parameters were identified, and the corresponding optimal inputs $\bar{u}_1$ and $\bar{u}_2$ were determined. The determination and the practical implementation method of the optimal control (singular mass ($\overline{m}$) and singular control ($\overline{u}$)) is presented in Appendix B–(B2). For modeling, relaxation and backwashing were assumed to have equivalent detachment effects, and their durations were adjusted proportionally to the experimental operation (Eq. (29)). For instance, the duration of the backwashing step in the optimal strategy (t_{BW}^{OC}) was calculated based on the ratio between the experimentally applied backwashing (t_{BW}^{TM}) and total physical cleaning durations (t_{PC}^{TM}).

$$t_{BW}^{OC} = \frac{t_{BW}^{TM}}{t_{PC}^{TM}} \cdot t_{PC}^{OC} \tag{29}$$

Where t_{PC}^{OC} is physical cleaning time for optimal control.

To evaluate the efficiency of the optimal control, two simulations were carried out until final time (t_F) corresponds to a total volume produced V_F (V_F = 1.914 m^3) as follows: i) #Run 1: the first determined control $\bar{u}_1$ = 0.61 –using transient phase model– is applied until V_F is reached; where $\bar{u}_1$ corresponds to a cycle of 8min5sF/32.5sR/50sBW/32.5sR, and ii) #Run 2: the second determined control $\bar{u}_2$ = 0,83 –using pseudo-steady-state phase data– is applied until V_F is reached; where $\bar{u}_2$ corresponds to a cycle of 9min10sF/14sR/22sBW/14sR.

Over time, a SEC_P was calculated to evaluate the performance of control strategies. For Run1, the SEC_P is initially slightly lower than that obtained with the classical strategy during the transient regime, indicating better energy performance at this early stage. However, as the system approached the pseudo-steady-state regime, this advantage disappeared and SEC_p eventually exceeded that of the classical strategy, showing that the optimal control derived from the transient regime does not ensure long-term energy efficiency. In contrast, Run2 initially exhibited a slightly higher SEC_p than the classical strategy, indicating lower short-term efficiency. However, SEC_p decreased more markedly over time, and under steady-state conditions, Run2 became more energy-efficient, ultimately achieving a lower SEC_p than the classical strategy.

For a total filtered volume of 1.914 m^3, the application of optimal control achieved a positive energy saving only for Run2 of 6.05% at the permeate pump compared to the classical strategy (Fig. 6(b)). By mitigating fouling, Run2 enabled the system to reach the target permeate volume 10 days earlier and increased the net permeate flux by nearly 20% due to shorter cleaning periods. Reduced backwashing frequency also lowered reagent use and membrane aging. However, the optimal strategy resulted in a lower NEB, as methane recovery decreased from 618 to 490 Wh·m^{-3}. The pumping energy saving (0.22 Wh·m^{-3}) remained negligible compared to the loss in recoverable methane energy (–128 Wh·m^{-3}).

In conclusion, the marked difference between the optimal control profiles $\bar{u}_1$ and $\bar{u}_2$ confirms that the optimal strategy evolves significantly from start-up to steady state. The long-term effectiveness of open-loop optimal control depends on system transient dynamics and model identification accuracy, supporting the need for an adaptive approach. Maximizing net energy recovery will ultimately require coupling biological and filtration dynamics.

4. Conclusion

This study aimed to develop and validate an integrated dynamic model for granular anaerobic membrane bioreactors, explicitly coupling biological processes, membrane fouling mechanisms, and filtration/backwash operations. Particular attention was given to the impact of cycle duration on fouling behavior and net energy performance. The modified AM2b model, which accounts for the return of detached solids during backwashing, accurately reproduced experimental trends for substrates, SMP, methane production, and TMP. Model predictions of fouling indicators showed good agreement with post-operation measurements, with relative errors below 17%. While the SEC_p remained nearly constant at around 120 Wh·m^{-3}, methane production and NEB were strongly influenced by cycle duration. Short filtration/backwash cycles (5–10 min) provided the best energy performance by limiting fouling while maintaining methane production. Finally, the application of optimal control proved effective in reducing SEC_p, and future work should focus on integrating methane production into the objective function.

CRediT authorship contribution statement

Aymen Chaaben: Writing – original draft, Visualization, Software, Methodology, Investigation, Formal analysis, Conceptualization. **Farshid Pajoum Shariati:** Writing – review & editing. **Geoffroy Lesage:** Writing – review & editing, Resources. **Jérôme Harmand:** Writing – review & editing, Supervision, Project administration, Methodology,

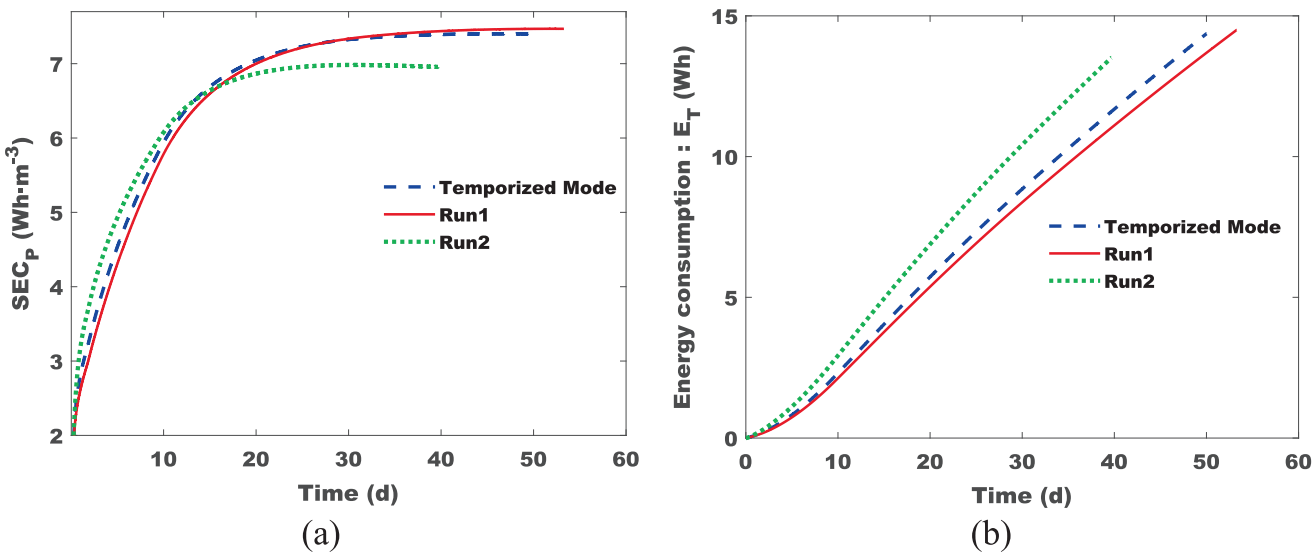

Fig. 6. Specific energy consumption of the permeate pump (SEC_P) corresponding to the cumulative energy consumption per cumulative permeate volume ($Wh \cdot m^{-3}$) (a), Cumulative Hydraulic pumping energy consumption (E_T) (Wh) (b), for Temporized Mode, Run1, and Run2 over time.

Funding acquisition. **Marc Heran:** Writing – review & editing, Validation, Supervision, Resources, Project administration, Funding acquisition.

Declaration of competing interest

The authors declare the following financial interests/personal relationships which may be considered as potential competing interests: Jerome Harmand reports financial support was provided by Agropolis Foundation. Marc Heran reports financial support was provided by Occitanie Region. If there are other authors, they declare that they have no known competing financial interests or personal relationships that could have appeared to influence the work reported in this paper.

Acknowledgments

The authors thank the REUSE research network (reuse.hub.inrae.fr), as well as the “Défi Clé Water Occitanie” and Labex Agro (AGROPOLIS Fondation) for the financial support of the WOc-WoD research project, which has partially funded this study.

Appendix A. Supplementary data

Supplementary data to this article can be found online at https://doi.org/10.1016/j.biortech.2026.134229.

Data availability

Data will be made available on request.

References

Abuabdou, S.M.A., Ahmad, W., Aun, N.C., Bashir, M.J.K., 2020. A review of anaerobic membrane bioreactors (AnMBR) for the treatment of highly contaminated landfill leachate and biogas production: Effectiveness, limitations and future perspectives. J. Clean. Prod. 255, 120215. https://doi.org/10.1016/j.jclepro.2020.120215.

Aichouche, F., Kalboussi, N., Rapaport, A., Harmand, J., 2020. Modeling and optimal control for production-regeneration systems - preliminary results -, in: 2020 European Control Conference (ECC). Presented at the 2020 European Control Conference (ECC), pp. 564–569. doi: 10.23919/ECC51009.2020.9143741.

Batstone, D.J., Keller, J., Angelidaki, I., Kalyuzhnyi, S.V., Pavlostathis, S.G., Rozzi, A., Sanders, W.T.M., Siegrist, H., Vavilin, V.A., 2002. The IWA Anaerobic Digestion Model No 1 (ADM1). Water Sci. Technol. 45, 65–73. https://doi.org/10.2166/wst.2002.0292.

Benyahia, B., Charfi, A., Lesage, G., Heran, M., Cherki, B., Harmand, J., 2024. Coupling a simple and Generic Membrane Fouling Model with Biological Dynamics: Application to the Modeling of an Anaerobic Membrane BioReactor (AnMBR). Membranes 14, 69. https://doi.org/10.3390/membranes14030069.

Bernard, O., Hadj-Sadok, Z., Dochain, D., Genovesi, A., Steyer, J.-P., 2001. Dynamical model development and parameter identification for an anaerobic wastewater treatment process. Biotechnol. Bioeng. 75, 424–438. https://doi.org/10.1002/bit.10036.

Chaaben, A., Ellouze, F., Ben Amar, N., Rapaport, A., Heran, M., Harmand, J., 2025. Evaluation of the Genericity of an Adaptive Optimal Control Approach to Optimize Membrane Filtration Systems. Membranes 15, 157. https://doi.org/10.3390/membranes15060157.

Chen, C., Liu, Z., Huang, X., 2020. 14 - Anaerobic membrane bioreactors for sustainable and energy-efficient municipal wastewater treatment, in: Ngo, H.H., Guo, W., Ng, H. Y., Mannina, G., Pandey, A. (Eds.), Current Developments in Biotechnology and Bioengineering. Elsevier, pp. 335–366. https://doi.org/10.1016/B978-0-12-819852-0.00014-2.

Cheng, H., Cheng, D., Mao, J., Lu, T., Hong, P.-Y., 2019. Identification and characterization of core sludge and biofilm microbiota in anaerobic membrane bioreactors. Environ. Int. 133, 105165. https://doi.org/10.1016/j.envint.2019.105165.

Das, S., O’Connell, M.G., Xu, H., Bernstein, R., Kim, J.-H., Sankhala, K., Segal-Peretz, T., Shevate, R., Zhang, W., Zhou, X., Darling, S.B., Dunn, J.B., 2022. Assessing advances in Anti-fouling Membranes to Improve Process Economics and Sustainability of Water Treatment. ACS EST Eng. 2, 2159–2173. https://doi.org/10.1021/acsestengg.2c00184.

Dong, H., Yue, L., Cheng, J., Xia, R., Zhou, J., 2022. Microbial electrochemical degradation of lipids for promoting methane production in anaerobic digestion. Bioresour. Technol. 345, 126467. https://doi.org/10.1016/j.biortech.2021.126467.

Drews, A., 2010. Membrane fouling in membrane bioreactors—Characterisation, contradictions, cause and cures. J. Membr. Sci. 363, 1–28. https://doi.org/10.1016/j.memsci.2010.06.046.

Du, X., Shi, Y., Jegatheesan, V., Haq, I.U., 2020. A Review on the Mechanism, Impacts and Control Methods of Membrane Fouling in MBR System. Membranes 10, 24. https://doi.org/10.3390/membranes10020024.

Duong, C.C., Chen, S.-S., Le, H.Q., Chang, H.-M., Nguyen, N.C., Cao, D.T.N., Chien, I.-C., 2020. A novel thermophilic anaerobic granular sludge membrane distillation bioreactor for wastewater reclamation. Environ. Sci. Pollut. Res. 27, 41751–41763. https://doi.org/10.1007/s11356-020-09987-4.

Gao, M., He, Q., Dong, H., Wang, J., Shi, J., Xie, C., Lo, Y.M., Zhao, L., 2022. Identification of the coupled fouling mechanism involved in microfiltration of tobacco extracts liquid by multistage Hermia model. J. Food Process Eng 45, e13961. https://doi.org/10.1111/jfpe.13961.

Gao, T., Jin, Y., Xiao, K., 2025. Techno–Economic and Environmental Impact Assessment of Membrane Bioreactors for Wastewater Treatment: a Review. Engineering. https://doi.org/10.1016/j.eng.2025.05.001.

Giménez, J.B., Martí, N., Ferrer, J., Seco, A., 2012. Methane recovery efficiency in a submerged anaerobic membrane bioreactor (SAnMBR) treating sulphate-rich urban wastewater: Evaluation of methane losses with the effluent. Bioresour. Technol. 118, 67–72. https://doi.org/10.1016/j.biortech.2012.05.019.

González, E., Díaz, O., Vera, L., Rodríguez-Gómez, L.E., Rodríguez-Sevilla, J., 2018. Feedback control system for filtration optimisation based on a simple fouling model dynamically applied to membrane bioreactors. J. Membr. Sci. 552, 243–252. https://doi.org/10.1016/j.memsci.2018.02.007.

Guo, G., Li, Y., Zhou, S., Chen, Y., Urasaki, K., Qin, Y., Kubota, K., Li, Y.-Y., 2022. Long term operation performance and membrane fouling mechanisms of anaerobic membrane bioreactor treating waste activated sludge at high solid concentration and high flux. Sci. Total Environ. 846, 157435. https://doi.org/10.1016/j.scitotenv.2022.157435.

Hamedi, H., Mohammadzadeh, O., Rasouli, S., Zendehboudi, S., 2021. A critical review of biomass kinetics and membrane filtration models for membrane bioreactor systems. J. Environ. Chem. Eng. 9, 106406. https://doi.org/10.1016/j.jece.2021.106406.

Harb, M., Xiong, Y., Guest, J., Amy, G., Hong, P.-Y., 2015. Differences in microbial communities and performance between suspended and attached growth anaerobic membrane bioreactors treating synthetic municipal wastewater. doi: 10.1039/C5EW00162E.

Ho, J., Sung, S., 2010. Methanogenic activities in anaerobic membrane bioreactors (AnMBR) treating synthetic municipal wastewater. Bioresour. Technol. 101, 2191–2196. https://doi.org/10.1016/j.biortech.2009.11.042.

Jang, H., Kang, S., Kim, J., 2024. Identification of Membrane Fouling with Greywater Filtration by Porous Membranes: combined effect of Membrane Pore size and Applied pressure. Membranes 14, 46. https://doi.org/10.3390/membranes14020046.

Jiménez-Benítez, A., Ruiz-Martínez, A., Ferrer, J., Ribes, J., Rogalla, F., Robles, A., 2023. Life cycle costing of AnMBR technology for urban wastewater treatment: a case study based on a demo-scale AnMBR system. J. Environ. Chem. Eng. 11, 110267. https://doi.org/10.1016/j.jece.2023.110267.

Jo, S.J., Kwon, H., Jeong, S.-Y., Lee, C.-H., Kim, T.G., 2016. Comparison of microbial communities of activated sludge and membrane biofilm in 10 full-scale membrane bioreactors. Water Res. 101, 214–225. https://doi.org/10.1016/j.watres.2016.05.042.

Kim, M., How, S.W., Dash, S.R., Wu, D., Kim, J., 2023. Membrane fouling, methane production and microbial community under fluidization of biocarrier with conductive surface in anaerobic fluidized bed membrane bioreactor for greywater treatment. J. Membr. Sci. 688, 122108. https://doi.org/10.1016/j.memsci.2023.122108.

Kong, Z., Li, L., Wu, J., Wang, T., Rong, C., Luo, Z., Pan, Y., Li, D., Li, Y., Huang, Y., Li, Y.-Y., 2021. Evaluation of bio-energy recovery from the anaerobic treatment of municipal wastewater by a pilot-scale submerged anaerobic membrane bioreactor (AnMBR) at ambient temperature. Bioresour. Technol. 339, 125551. https://doi.org/10.1016/j.biortech.2021.125551.

Layer, M., Adler, A., Reynaert, E., Hernandez, A., Pagni, M., Morgenroth, E., Holliger, C., Derlon, N., 2019. Organic substrate diffusibility governs microbial community composition, nutrient removal performance and kinetics of granulation of aerobic granular sludge. Water Res. X 4, 100033. https://doi.org/10.1016/j.wroa.2019.100033.

Lei, Z., Yang, S., Li, Y., Wen, W., Wang, X.C., Chen, R., 2018. Application of anaerobic membrane bioreactors to municipal wastewater treatment at ambient temperature: a review of achievements, challenges, and perspectives. Bioresour. Technol. 267, 756–768. https://doi.org/10.1016/j.biortech.2018.07.050.

Li, Y., Ren, Y., Ji, J., Li, Y.-Y., Kobayashi, T., 2023. Anaerobic Membrane Bioreactors for Municipal Wastewater Treatment, Sewage Sludge Digestion and Biogas Upgrading: a Review. Sustainability 15, 15129. https://doi.org/10.3390/su152015129.

Lipps, W.C., Braun-Howland, E.B., Baxter, T.E., 2023. Standard Methods for the Examination of Water and Wastewater. American Public Health Association.

Smith, L., Skerlos, S., Raskin, L., 2015. Anaerobic membrane bioreactor treatment of domestic wastewater at psychrophilic temperatures ranging from 15 °C to 3 °C. Environ. Sci. Water Res. Technol. 1, 56–64. https://doi.org/10.1039/C4EW00070F.

Maaz, M., Yasin, M., Aslam, M., Kumar, G., Atabani, A.E., Idrees, M., Anjum, F., Jamil, F., Ahmad, R., Khan, A.L., Lesage, G., Heran, M., Kim, J., 2019. Anaerobic membrane bioreactors for wastewater treatment: Novel configurations, fouling control and energy considerations. Bioresour. Technol. 283, 358–372. https://doi.org/10.1016/j.biortech.2019.03.061.

Mannina, G., Alliet, M., Brepols, C., Comas, J., Harmand, J., Heran, M., Kalboussi, N., Makinia, J., Robles, Á., Rebouças, T.F., Ni, B.-J., Rodriguez-Roda, I., Victoria Ruano, M., Bertanza, G., Smets, I., 2021. Integrated membrane bioreactors modelling: a review on new comprehensive modelling framework. Bioresour. Technol. 329, 124828. https://doi.org/10.1016/j.biortech.2021.124828.

Martin, I., Pidou, M., Soares, A., Judd, S., Jefferson, B., 2011. Modelling the energy demands of aerobic and anaerobic membrane bioreactors for wastewater treatment. Environ. Technol. 32, 921–932. https://doi.org/10.1080/09593330.2011.565806.

Poorasgari, E., Vistisen Bugge, T., Lykkegaard Christensen, M., Koustrup Jørgensen, M., 2015. Compressibility of fouling layers in membrane bioreactors. J. Membr. Sci. 475, 65–70. https://doi.org/10.1016/j.memsci.2014.09.056.

Ramakrishnan, A., Surampalli, R.Y., 2012. Comparative performance of UASB and anaerobic hybrid reactors for the treatment of complex phenolic wastewater. Bioresour. Technol. 123, 352–359. https://doi.org/10.1016/j.biortech.2012.07.072.

Robles, Á., Ruano, M.V., Charfi, A., Lesage, G., Heran, M., Harmand, J., Seco, A., Steyer, J.-P., Batstone, D.J., Kim, J., Ferrer, J., 2018. A review on anaerobic membrane bioreactors (AnMBRs) focused on modelling and control aspects. Bioresour. Technol. 270, 612–626. https://doi.org/10.1016/j.biortech.2018.09.049.

Sanchez, L., Carrier, M., Cartier, J., Charmette, C., Heran, M., Steyer, J.-P., Lesage, G., 2022. Enhanced organic degradation and biogas production of domestic wastewater at psychrophilic temperature through submerged granular anaerobic membrane bioreactor for energy-positive treatment. Bioresour. Technol. 353, 127145. https://doi.org/10.1016/j.biortech.2022.127145.

Sanchez, L., Vinardell, S., Charreton, J., Heran, M., Lesage, G., 2023. Assessing the impact of granular anaerobic membrane bioreactor intensification on treatment performance, membrane fouling and economic balance. J. Environ. Chem. Eng. 11, 109369. https://doi.org/10.1016/j.jece.2023.109369.

Sanchis-Perucho, P., Harmand, J., Feddaoui-papin, A., Aguado, D., Robles, Á., 2024. Building a simple multivariable filtration model to predict irreversible fouling when directly filtering municipal wastewater. J. Environ. Chem. Eng. 12, 112653. https://doi.org/10.1016/j.jece.2024.112653.

Seib, M.D., Berg, K.J., Zitomer, D.H., 2016. Low energy anaerobic membrane bioreactor for municipal wastewater treatment. J. Membr. Sci. 514, 450–457. https://doi.org/10.1016/j.memsci.2016.05.007.

Shao, Z., Gnanasekar, P., Tratnik, N., Tanguy, N.R., Guo, X., Zhu, M., Qiu, L., Yan, N., Chen, H., 2023. Low-temperature torrefaction assisted with solid-state KOH/urea pretreatment for accelerated methane production in wheat straw anaerobic digestion. Bioresour. Technol. 377, 128940. https://doi.org/10.1016/j.biortech.2023.128940.

Sohn, W., Jiang, J., Su, Z., Zheng, M., Wang, Q., Phuntsho, S., Kyong Shon, H., 2024. Microbial community analysis of membrane bioreactor incorporated with biofilm carriers and activated carbon for nitrification of urine. Bioresour. Technol. 397, 130462. https://doi.org/10.1016/j.biortech.2024.130462.

Tomczak, W., Gryta, M., Grubecki, I., Miłek, J., 2023. Biogas Production in AnMBRs via Treatment of municipal and Domestic Wastewater: Opportunities and Fouling Mitigation strategies. Appl. Sci. 13, 6466. https://doi.org/10.3390/app13116466.

Uman, A.E., Bair, R.A., Yeh, D.H., 2021. Assessment of an Anaerobic Membrane Bioreactor (AnMBR) Treating Medium-Strength Synthetic Wastewater under Cyclical Membrane operation. Membranes 11, 415. https://doi.org/10.3390/membranes11060415.

Vinardell, S., Astals, S., Peces, M., Cardete, M.A., Fernández, I., Mata-Alvarez, J., Dosta, J., 2020. Advances in anaerobic membrane bioreactor technology for municipal wastewater treatment: a 2020 updated review. Renew. Sustain. Energy Rev. 130, 109936. https://doi.org/10.1016/j.rser.2020.109936.

Zielińska, M., Ojo, A., 2023. Anaerobic Membrane Bioreactors (AnMBRs) for Wastewater Treatment: Recovery of Nutrients and Energy, and Management of Fouling. Energies 16, 2829. https://doi.org/10.3390/en16062829.